DYNAMIC ANALYSIS AND OPTIMISATION OF A KINEMATICALLY-REDUNDANT PLANAR PARALLEL MANIPULATOR

Roger Boudreau[1], Jérémie Léger[2], Hakim Tinaou[1], André Gallant[3]
[1]*Département de génie mécanique, Université de Moncton, Moncton, NB, Canada*
E-mail: roger.a.boudreau@umoncton.ca
[2]*Département de génie mécanique, École de Technologie Supérieure, Montréal, Qc, Canada*
[3]*Département de génie mécanique, Université Laval, Québec, Qc, Canada*

ABSTRACT

This paper presents the dynamic model of a kinematically-redundant planar parallel manipulator and an optimisation method to minimise the actuator torques when the end-effector is subjected to a wrench while following a trajectory. A previous study proposed a kinetostatic approach to solve the same problem. The objective of the work presented here was to verify if the kinetostatic assumption was valid. The inclusion of the dynamic model in the optimisation produced some undesirable oscillations and required the use of a different objective function. It is shown that for the application considered, the kinetostatic approach provided an acceptable solution.

Keywords: planar parallel manipulators; kinematic redundancy; dynamic analysis; optimisation.

ANALYSE DYNAMIQUE ET OPTIMISATION D'UN MANIPULATEUR PARALLÈLE PLAN AVEC REDONDANCE CINÉMATIQUE

RÉSUMÉ

Ce travail présente le modèle dynamique d'un manipulateur parallèle plan avec redondance cinématique et une méthode pour optimiser les couples des actionneurs lorsque l'organe terminal est soumis à un torseur en suivant une trajectoire. Une étude précédente proposait la solution du même problème en supposant une analyse statique. Le but de ce travail était de vérifier si cette supposition était valide. Lorsque le modèle dynamique est inclus dans l'optimisation, des oscillations indésirables se produisent et une fonction objectif différente doit être utilisée. Il est démontré que pour l'exemple étudié, l'approche statique produisait une solution acceptable.

Mots-clés : manipulateurs parallèles plans; redondance cinématique; analyse dynamique; optimisation.

INTRODUCTION

Parallel manipulators have certain advantages over serial manipulators, such as a larger payload-to-weight ratio and higher stiffness. However, their workspaces are smaller and usually contain a large number of Type-2 singular configurations [1] in which they cannot sustain a wrench applied to the end effector. Different types of redundancy have been proposed to reduce or eliminate these singularities. Actuation redundancy consists of actuating a normally passive joint in one or more branches of the manipulator [e.g. 2,3], or of adding an extra actuated branch or branches to a manipulator [e.g. 4,5]; the latter is sometimes called branch redundancy. When there is actuation redundancy, there exists an infinity of solutions for the actuator torques to sustain a wrench. On the other hand, kinematic redundancy consists of adding extra joints and links to the manipulator [e.g. 6-12], and it can also reduce or eliminate singularities. In this case, there exists an infinity of solutions to the inverse displacement problem.

In [13], kinematic redundancy was used to optimise the actuator forces of a planar 3-PRPR[1] [14] parallel manipulator when its end-effector was subjected to a wrench following different trajectories. It was assumed that the end-effector was moving slowly, as in a machining operation, and a kinetostatic approach was considered. The optimisation showed that the forces required by the kinematically-redundant manipulator were lower than those of the non-redundant 3-RPR manipulator. In particular, the kinematically-redundant manipulator could pass through configurations that were singular for the non-redundant manipulator. Even if the end-effector velocity was slow, i.e., 0.005 m/s, and the actuator velocities were constrained to be between ±0.15 m/s, the actuator accelerations were sometimes larger than 4 m/s^2. This paper includes the dynamic effects to verify if the kinetostatic assumption was valid.

The paper is organised as follows. The manipulators studied are first described. A kinematic analysis is then presented, followed by a dynamic analysis based on the Newton-Euler approach. The optimisation procedure used is explained, followed by results and conclusions.

1 DESCRIPTION OF THE MANIPULATOR

The 3-PRPR shown in Fig. 1 is similar to the well-known 3-RPR manipulator, except for an extra actuated prismatic joint (base prismatic joint) added to each leg between points O_i and A_i, i =*1,2,3,* that are fixed to the base and cannot rotate. All three of these actuators are aligned along the lines formed by the equilateral triangle generated from the base points O_i. A fixed reference frame is attached to the base centre at point O and a mobile reference frame is attached to the end-effector centre at point P. The orientation angle φ of the end effector is defined by the angle formed between the X and x axes. The prismatic actuators between points A_i and B_i are henceforth called the distal prismatic joints. While i denotes the leg number, j denotes the actuator's placement in the leg. Note that the 3-RPR manipulator with which the results will be compared is obtained when ρ_{i1} is set to zero and points A_i become fixed and coincident with points O_i.

In order to model the dynamic equations, a leg i is shown in Fig. 2. Each prismatic joint is comprised of a cylinder and a piston. The mass of the piston of the base prismatic joint is designated by m_1, while the mass and the moment of inertia with respect to its centre of mass of the cylinder of the distal link and of the piston of the distal link are denoted by m_2, I_2 and m_3, I_3, respectively. The centres of mass are shown in the middle of the members. Parameter r_2 is the distance between the centre of gravity G_{2i} and A_i while L_3 is the length of the distal piston members. Note that the mass and moment of inertia of the fixed cylinder of the base link have no effect on the dynamic equations. The mass of the platform is denoted as m_p and its moment of inertia with respect to its centre of mass as I_p. The extremity of the piston of the base link is

[1] The first number of the nomenclature indicates the number of branches, while revolute and prismatic joints are denoted by R and P, respectively. Actuated joints are underlined while the others are passive.

attached to the cylinder of the distal link. The "overhang" in the cylinder of the distal link is to allow a longer stroke.

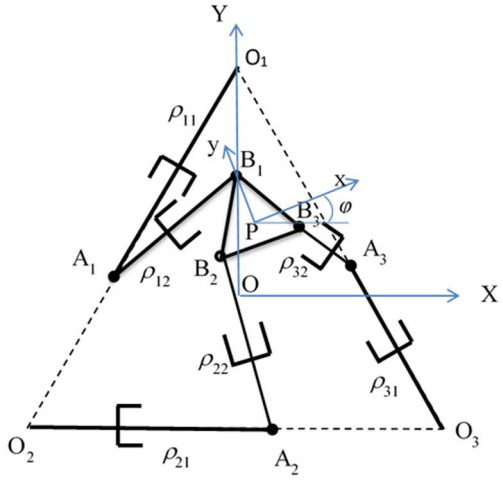

Fig. 1. 3-PRPR manipulator.

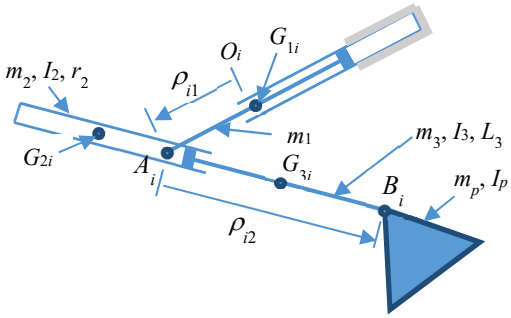

Fig. 2. Detailed leg of 3-PRPR manipulator.

2 KINEMATIC ANALYSIS

2.1 Velocity Analysis

The kinematic analysis of the 3-PRPR manipulator is derived in sections 2.1 and 2.2. From Fig. 1, the vector loop equation can be written as

$$\mathbf{OO}_i + \mathbf{O}_i\mathbf{A}_i + \mathbf{A}_i\mathbf{B}_i = \mathbf{OP} + \mathbf{PB}_i \tag{1}$$

$$\mathbf{OO}_i + \rho_{i1}\mathbf{n}_{i1} + \rho_{i2}\mathbf{n}_{i2} = \mathbf{OP} + \mathbf{PB}_i \tag{2}$$

where $\mathbf{n}_{i1}$ and $\mathbf{n}_{i2}$ represent unit vectors along the base link from O_i to A_i and along the distal link from A_i to B_i, respectively. The derivative with respect to time of $\mathbf{n}_{i2}$ and $\mathbf{PB}_i$ produces the following quantities:

$$\dot{\mathbf{n}}_{i2} = \dot{\theta}_{i2}(\mathbf{k} \times \mathbf{n}_{i2}) \tag{3}$$

$$\dot{\mathbf{PB}}_i = \dot{\varphi}(\mathbf{k} \times \mathbf{PB}_i) \tag{4}$$

where $\dot{\theta}_{i2}$ and $\dot{\varphi}$ are the angular velocities of the distal link i and of the end effector, respectively, and $\mathbf{k}$ is the unit vector pointing in the Z direction.

The derivative with respect to time of Eq. (2) yields

$$\dot{\rho}_{i1}\mathbf{n}_{i1} + \dot{\rho}_{i2}\mathbf{n}_{i2} + \rho_{i2}\dot{\theta}_{i2}(\mathbf{k} \times \mathbf{n}_{i2}) = \mathbf{V}_G + \dot{\varphi}(\mathbf{k} \times \mathbf{PB}_i) \tag{5}$$

Angular velocity $\dot{\theta}_{i2}$ can be eliminated by a dot multiplication with $\mathbf{n}_{i2}$.

$$\dot{\rho}_{i1}\mathbf{n}_{i2} \cdot \mathbf{n}_{i1} + \dot{\rho}_{i2} = \mathbf{n}_{i2} \cdot \mathbf{V}_G + \dot{\varphi}\mathbf{n}_{i2} \cdot (\mathbf{k} \times \mathbf{PB}_i) \tag{6}$$

The last term can be rearranged as $\dot{\varphi}\mathbf{k} \cdot (\mathbf{PB}_i \times \mathbf{n}_{i2})$. Eq. (6) becomes

$$\dot{\rho}_{i2} = \mathbf{n}_{i2} \cdot \mathbf{V}_G + \dot{\varphi}\mathbf{k} \cdot (\mathbf{PB}_i \times \mathbf{n}_{i2}) - \dot{\rho}_{i1}\mathbf{n}_{i2} \cdot \mathbf{n}_{i1} \tag{7}$$

Multiplying Eq. (7) by ρ_{i2} and noting that $\rho_{i2}\mathbf{n}_{i2} = \mathbf{B}_i - \mathbf{A}_i$, the velocity equation in matrix form for all the legs gives

$$\mathbf{J}_q\dot{\mathbf{q}} = \mathbf{J}_x\dot{\mathbf{x}} \tag{8}$$

where

$$\mathbf{J}_q = \begin{bmatrix} \mathbf{n}_{11}^{\mathrm{T}} \cdot (\mathbf{B}_1 - \mathbf{A}_1) & \rho_{12} & 0 & 0 & 0 & 0 \\ 0 & 0 & \mathbf{n}_{21}^{\mathrm{T}} \cdot (\mathbf{B}_2 - \mathbf{A}_2) & \rho_{22} & 0 & 0 \\ 0 & 0 & 0 & 0 & \mathbf{n}_{31}^{\mathrm{T}} \cdot (\mathbf{B}_3 - \mathbf{A}_3) & \rho_{32} \end{bmatrix} \tag{9}$$

$$\mathbf{J}_x = \begin{bmatrix} (\mathbf{B}_1 - \mathbf{A}_1)^{\mathrm{T}} & \mathbf{k}^{\mathrm{T}} \cdot \mathbf{PB}_1 \times (\mathbf{B}_1 - \mathbf{A}_1) \\ (\mathbf{B}_2 - \mathbf{A}_2)^{\mathrm{T}} & \mathbf{k}^{\mathrm{T}} \cdot \mathbf{PB}_2 \times (\mathbf{B}_2 - \mathbf{A}_2) \\ (\mathbf{B}_3 - \mathbf{A}_3)^{\mathrm{T}} & \mathbf{k}^{\mathrm{T}} \cdot \mathbf{PB}_3 \times (\mathbf{B}_3 - \mathbf{A}_3) \end{bmatrix} \tag{10}$$

The vector of actuated joint velocities is given by $\dot{\mathbf{q}} = [\dot{\rho}_{11}\ \dot{\rho}_{12}\ \dot{\rho}_{21}\ \dot{\rho}_{22}\ \dot{\rho}_{31}\ \dot{\rho}_{32}]^{\mathrm{T}}$ while the vector of the end effector's velocity and angular velocity is $\dot{\mathbf{x}} = [\dot{x}\ \ \dot{y}\ \dot{\varphi}]^{\mathrm{T}}$.

Angular velocity $\dot{\theta}_{i2}$ can be obtained by cross multiplying Eq. (5) with vector $\mathbf{n}_{i2}$.

$$\dot{\rho}_{i1}\mathbf{n}_{i2} \times \mathbf{n}_{i1} + \rho_{i2}\dot{\theta}_{i2}\mathbf{n}_{i2} \times (\mathbf{k} \times \mathbf{n}_{i2}) = \mathbf{n}_{i2} \times \mathbf{V}_G + \dot{\varphi}\mathbf{n}_{i2} \times (\mathbf{k} \times \mathbf{PB}_i) \tag{11}$$

where

$$\mathbf{n}_{i2} \times \mathbf{n}_{i1} = \left(n_{i2_x}n_{i1_y} - n_{i2_y}n_{i1_x}\right)\mathbf{k} \tag{12}$$

$$\mathbf{n}_{i2} \times (\mathbf{k} \times \mathbf{n}_{i2}) = \mathbf{k} \tag{13}$$

$$\mathbf{n}_{i2} \times \mathbf{V}_G = \left(n_{i2_x}\dot{y} - n_{i2_y}\dot{x}\right)\mathbf{k} \tag{14}$$

$$\mathbf{n}_{i2} \times (\mathbf{k} \times \mathbf{PB}_i) = \mathbf{k}(\mathbf{n}_{i2} \cdot \mathbf{PB}_i) - \mathbf{PB}_i(\mathbf{n}_{i2} \cdot \mathbf{k}) = \mathbf{k}(\mathbf{n}_{i2} \cdot \mathbf{PB}_i) \tag{15}$$

Since all the components are about the z axis, Eq. (11) becomes

$$\dot{\theta}_{i2} = \frac{1}{\rho_{i2}}\left(\begin{bmatrix} -n_{i2_y} & n_{i2_x} & \mathbf{n}_{i2} \cdot \mathbf{PB}_i \end{bmatrix}\begin{bmatrix} \dot{x} \\ \dot{y} \\ \dot{\varphi} \end{bmatrix} - \dot{\rho}_{i1}\left(n_{i2_x}n_{i1_y} - n_{i2_y}n_{i1_x}\right)\right) \tag{16}$$

2.2 Acceleration Analysis

The derivative with respect to time of Eq. (5) yields

$$\ddot{\rho}_{i1}\mathbf{n}_{i1} + \ddot{\rho}_{i2}\mathbf{n}_{i2} + \dot{\rho}_{i2}\dot{\theta}_{i2}(\mathbf{k} \times \mathbf{n}_{i2}) + \dot{\rho}_{i2}\dot{\theta}_{i2}(\mathbf{k} \times \mathbf{n}_{i2}) + \rho_{i2}\ddot{\theta}_{i2}(\mathbf{k} \times \mathbf{n}_{i2}) + \rho_{i2}\dot{\theta}_{i2}\left(\mathbf{k} \times \dot{\theta}_{i2}(\mathbf{k} \times \mathbf{n}_{i2})\right) = \mathbf{a}_G + \ddot{\varphi}(\mathbf{k} \times \mathbf{PB}_i) + \dot{\varphi}(\mathbf{k} \times \dot{\varphi}(\mathbf{k} \times \mathbf{PB}_i)) \tag{17}$$

where

$$\mathbf{k} \times (\mathbf{k} \times \mathbf{n}_{i2}) = -\mathbf{n}_{i2} \tag{18}$$

$$\mathbf{k} \times (\mathbf{k} \times \mathbf{PB}_i) = -\mathbf{PB}_i \tag{19}$$

Equation (17) becomes

$$\ddot{\rho}_{i1}\mathbf{n}_{i1} + \ddot{\rho}_{i2}\mathbf{n}_{i2} + 2\dot{\rho}_{i2}\dot{\theta}_{i2}(\mathbf{k} \times \mathbf{n}_{i2}) + \rho_{i2}\ddot{\theta}_{i2}(\mathbf{k} \times \mathbf{n}_{i2}) - \rho_{i2}\dot{\theta}_{i2}^2\mathbf{n}_{i2} = \mathbf{a}_G + \ddot{\varphi}(\mathbf{k} \times \mathbf{PB}_i) - \dot{\varphi}^2\mathbf{PB}_i \tag{20}$$

The third and fourth terms on the left hand side of Eq. (20) can be eliminated by dot multiplication with $\mathbf{n}_{i2}$.

$$\ddot{\rho}_{i1}\mathbf{n}_{i2} \cdot \mathbf{n}_{i1} + \ddot{\rho}_{i2} - \rho_{i2}\dot{\theta}_{i2}^2 = \mathbf{n}_{i2} \cdot \mathbf{a}_G + \ddot{\varphi}\mathbf{n}_{i2} \cdot (\mathbf{k} \times \mathbf{PB}_i) - \dot{\varphi}^2\mathbf{n}_{i2} \cdot \mathbf{PB}_i \tag{21}$$

The acceleration of the distal prismatic joint is thus

$$\ddot{\rho}_{i2} = \mathbf{n}_{i2} \cdot \mathbf{a}_G + \ddot{\varphi}\mathbf{k} \cdot (\mathbf{PB}_i \times \mathbf{n}_{i2}) - \dot{\varphi}^2\mathbf{n}_{i2} \cdot \mathbf{PB}_i + \rho_{i2}\dot{\theta}_{i2}^2 - \ddot{\rho}_{i1}\mathbf{n}_{i2} \cdot \mathbf{n}_{i1} \tag{22}$$

The angular acceleration of distal link *i* can be obtained by cross multiplying $\mathbf{n}_{i2}$ with Eq. (20).

$$\ddot{\rho}_{i1}\mathbf{n}_{i2}\times\mathbf{n}_{i1}+2\dot{\rho}_{i2}\dot{\theta}_{i2}\mathbf{n}_{i2}\times(\mathbf{k}\times\mathbf{n}_{i2})+\rho_{i2}\ddot{\theta}_{i2}\mathbf{n}_{i2}\times(\mathbf{k}\times\mathbf{n}_{i2})= \mathbf{n}_{i2}\times\mathbf{a}_G+\ddot{\varphi}\mathbf{n}_{i2}\times(\mathbf{k}\times\mathbf{PB_i})-\dot{\varphi}^2\mathbf{n}_{i2}\times\mathbf{PB_i} \quad (23)$$

Substituting the results of Eqs. (13) and (15) into Eq. (23) yields

$$\ddot{\rho}_{i1}\mathbf{n}_{i2}\times\mathbf{n}_{i1}+2\dot{\rho}_{i2}\dot{\theta}_{i2}\mathbf{k}+\rho_{i2}\ddot{\theta}_{i2}\mathbf{k}=\mathbf{n}_{i2}\times\mathbf{a}_G+\ddot{\varphi}\mathbf{k}(\mathbf{n}_{i2}\cdot\mathbf{PB_i})-\dot{\varphi}^2\mathbf{n}_{i2}\times\mathbf{PB_i} \quad (24)$$

Collecting the $\mathbf{k}$ components yields

$$\ddot{\rho}_{i1}\left(n_{i2_x}n_{i1_y}-n_{i2_y}n_{i1_x}\right)+2\dot{\rho}_{i2}\dot{\theta}_{i2}+\rho_{i2}\ddot{\theta}_{i2}= \left(n_{i2_x}\ddot{y}-n_{i2_y}\ddot{x}\right)+\ddot{\varphi}(\mathbf{n}_{i2}\cdot\mathbf{PB_i})-\dot{\varphi}^2\left(n_{i2_x}PB_{i_y}-n_{i2_y}PB_{i_x}\right) \quad (25)$$

The angular acceleration of the distal link is thus

$$\ddot{\theta}_{i2}=\frac{1}{\rho_{i2}}\left(\begin{bmatrix}-n_{i2_y} & n_{i2_x} & \mathbf{n}_{i2}\cdot\mathbf{PB_i}\end{bmatrix}\begin{bmatrix}\ddot{x}\\ \ddot{y}\\ \ddot{\varphi}\end{bmatrix}-\ddot{\rho}_{i1}\left(n_{i2_x}n_{i1_y}-n_{i2_y}n_{i1_x}\right) -\dot{\varphi}^2\left(n_{i2_x}PB_{i_y}-n_{i2_y}PB_{i_x}\right)-2\dot{\rho}_{i2}\dot{\theta}_{i2}\right) \quad (26)$$

The Newton-Euler approach is used here to obtain the dynamic equations of the manipulator, therefore the accelerations of the centres of mass of the moving links must be determined. The acceleration of the mass m_1 is $\ddot{\rho}_{i1}$ (Fig. 2). Let $\mathbf{r}_{G2i}$ and $\mathbf{r}_{G3i}$ denote the position vectors of the centres of mass of the cylinder and of the piston of the distal link i with respect to A_i, respectively. The position of the centre of mass of the distal cylinder of leg i is

$$\mathbf{x}_{G_{2i}}=\mathbf{OO}_i+\mathbf{O}_i\mathbf{A}_i+\mathbf{r}_{G2i}=\mathbf{OO}_i+\rho_{i1}\mathbf{n}_{i1}-r_{G2i}\mathbf{n}_{i2} \quad (27)$$

where r_{G2i} is the constant amplitude of the vector $\mathbf{r}_{G2i}$ and is in the negative direction of $\mathbf{n}_{i2}$. The derivative with respect to time yields

$$\mathbf{v}_{G_{2i}}=\dot{\rho}_{i1}\mathbf{n}_{i1}-r_{G2i}\dot{\theta}_{i2}(\mathbf{k}\times\mathbf{n}_{i2}) \quad (28)$$

The acceleration becomes

$$\mathbf{a}_{G_{2i}}=\ddot{\rho}_{i1}\mathbf{n}_{i1}-r_{G2i}\ddot{\theta}_{i2}(\mathbf{k}\times\mathbf{n}_{i2})-r_{G2i}\dot{\theta}_{i2}\big(\mathbf{k}\times\dot{\theta}_{i2}(\mathbf{k}\times\mathbf{n}_{i2})\big) \quad (29)$$

To simplify the notation, let $\mathbf{n}_{i2_\perp}$ denote the cross product $\mathbf{k}\times\mathbf{n}_{i2}$, i.e. a unit vector perpendicular to $\mathbf{n}_{i2}$ rotated 90 degrees in the counter clockwise direction. Equation (29) simplifies to

$$\mathbf{a}_{G_{2i}}=\ddot{\rho}_{i1}\mathbf{n}_{i1}-r_{G2i}\ddot{\theta}_{i2}\mathbf{n}_{i2_\perp}+r_{G2i}\dot{\theta}_{i2}^2\mathbf{n}_{i2} \quad (30)$$

where all the terms have been previously found. Assuming that the centre of mass of the piston of the distal link of leg i is in the middle of the rod, the amplitude of its position vector and its derivatives with respect to time are

$$r_{G3i}=\rho_{i2}-\frac{L_3}{2} \quad (31)$$

$$\dot{r}_{G3i}=\dot{\rho}_{i2} \quad (32)$$

$$\ddot{r}_{G3i}=\ddot{\rho}_{i2} \quad (33)$$

The acceleration of the centre of mass of the piston of the distal link of leg i is found similarly, noting that $\mathbf{r}_{G3i}$ will be in the positive $\mathbf{n}_{i2}$ direction, and

$$\mathbf{x}_{G_{3i}}=\mathbf{OO}_i+\rho_{i1}\mathbf{n}_{i1}+r_{G3i}\mathbf{n}_{i2} \quad (34)$$

$$\mathbf{v}_{G_{3i}}=\dot{\rho}_{i1}\mathbf{n}_{i1}+\dot{\rho}_{i2}\mathbf{n}_{i2}+r_{G3i}\dot{\theta}_{i2}(\mathbf{k}\times\mathbf{n}_{i2}) \quad (35)$$

Taking the derivative with respect to time and simplifying yields

$$\mathbf{a}_{G_{3i}}=\ddot{\rho}_{i1}\mathbf{n}_{i1}+\left(\ddot{\rho}_{i2}-r_{G3i}\dot{\theta}_{i2}^2\right)\mathbf{n}_{i2}+\left(2\dot{\rho}_{i2}\dot{\theta}_{i2}+r_{G3i}\ddot{\theta}_{i2}\right)\mathbf{n}_{i2_\perp} \quad (36)$$

3 NEWTON-EULER FORMULATION

With the results of the preceding section, all the accelerations of the centres of mass and the angular accelerations of each link can be computed. Figure 3 shows the force analysis diagrams for the manipulator. Inertial forces and moments are not shown. From Fig. 3(b), the sum of moments about A_i yields

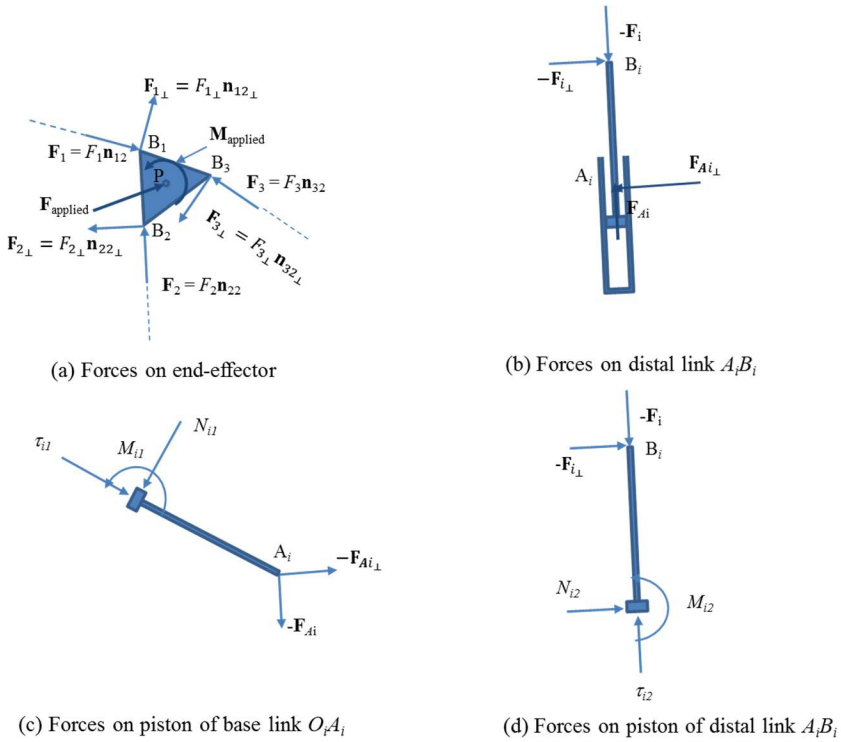

Fig. 3. Forces acting on end effector and links.

$$-F_{i_\perp}\rho_{2i} = (I_2 + I_3)\ddot{\theta}_{i2} - r_{G2i}\mathbf{n}_{i2} \times m_2\mathbf{a}_{G_{2i}} + r_{G3i}\mathbf{n}_{i2} \times m_3\mathbf{a}_{G_{3i}} \tag{37}$$

from which $F_{i_\perp}$ can be computed. From Fig. 3(a), the sum of forces and sum of moments about P on the platform yields

$$\sum_{i=1}^{3} F_i\,\mathbf{n}_{i2} + \sum_{i=1}^{3} F_{i_\perp}\,\mathbf{n}_{i2_\perp} + \mathbf{F}_{\text{applied}} = m_p\mathbf{a}_G$$
$$\sum_{i=1}^{3} \mathbf{PB}_i \times \left(F_i\mathbf{n}_{i2} + F_{i_\perp}\mathbf{n}_{i2_\perp}\right) + M_{\text{applied}}\mathbf{k} = I_p\ddot{\phi}\mathbf{k} \tag{38}$$

where $\mathbf{F}_{\text{applied}}$ is an external force and M_{applied} is the amplitude of an external moment applied to the platform, respectively. The three equations in (38) have three unknowns, allowing the determination of F_i, $i = 1, 2, 3$. The actuator forces in the distal links can be obtained from a sum of forces along the directions of the pistons as shown in Fig. 3(d).

$$\tau_{i2} = F_i + m_3\mathbf{a}_{G_{3i}} \cdot \mathbf{n}_{i2} \tag{39}$$

To determine the actuator forces in the base links, consider Fig. 3(b). Let $\mathbf{F}_i = F_i\mathbf{n}_{i2} + F_{i_\perp}\mathbf{n}_{i2_\perp}$. The total force at A_i, F_{Ai} can be obtained by the sum of forces on the distal link

$$\mathbf{F}_{Ai} - \mathbf{F}_i = m_2\mathbf{a}_{G_{2i}} + m_3\mathbf{a}_{G_{3i}} \tag{40}$$

From Fig. 3(c), the actuator forces in the base links can be determined.

$$\tau_{i1} - \mathbf{F}_{Ai} \cdot \mathbf{n}_{i1} = m_1\mathbf{a}_{G_{1i}} \cdot \mathbf{n}_{i1} \tag{41}$$

For a given pose with a specified velocity and acceleration, the inverse displacement problem has an infinite number of solutions. When the position, velocity and acceleration of the base actuator are specified, the velocities and accelerations of the distal actuators can be computed from Eqs. (7) and (22), respectively, while the angular velocities and angular accelerations of the distal links can be computed using Eqs. (16) and (26), respectively. These quantities can be used to compute the accelerations of the centres of mass of the cylinder and piston of distal link i with Eqs. (30) and (36), respectively. All the quantities required to compute the actuation forces are thus known.

4 OPTIMISATION PROCEDURE

The infinite number of possible solutions to the inverse displacement problem for a given trajectory enables the minimisation of the joint forces and singularity avoidance when the kinematically-redundant manipulator is considered [13]. At each point of the trajectory, an optimal value was found for the base prismatic joint vector containing the lengths of each base joint (ρ_{i1} for $i = 1,2,3$). Optimal values were found with Sequential Quadratic Programming (SQP) by the use of Matlab's *fmincon* function in the optimisation toolbox. These optimised values were then used as an initial guess for the next trajectory point. For the first initial guess, the values that minimised $\boldsymbol{\tau}^T\boldsymbol{\tau}$ at the initial pose were found using Particle Swarm Optimisation (PSO). Constraints on the joint displacements as well as on the maximum velocity were implemented. For the kinetostatic analysis, the optimisation problem was formulated as:

$$\min_{\rho_{i1}} \boldsymbol{\tau}^T\boldsymbol{\tau} \tag{42}$$

subject to:

$$\rho_{ij_{min}} \leq \rho_{ij} \leq \rho_{ij_{max}} \tag{43}$$

$$-\dot{\rho}_{ij_{max}} \leq \dot{\rho}_{ij} \leq \dot{\rho}_{ij_{max}} \tag{44}$$

where $i = 1,2,3$, $j = 1,2$ and $\boldsymbol{\tau}$ is the vector of actuator forces of all six actuators.

When optimisations were performed including the dynamics of the manipulator, the results were very unstable and undesirable oscillations occurred in the solutions. To remove these oscillations, the objective function was modified based on results proposed in [15], and a term was added to limit the angular accelerations of the distal links.

$$\min_{\rho_{i1}} \boldsymbol{\tau}^T\boldsymbol{\tau} + \alpha\left(b\left\|\ddot{\theta}_{i2}\right\|_2^2 + (1-b)\left\|\ddot{\theta}_{i2}\right\|_\infty\right) \tag{45}$$

where α and b are constants and $\left\|\ddot{\theta}_{i2}\right\|_2^2$ and $\left\|\ddot{\theta}_{i2}\right\|_\infty$ are the two-norm squared and the infinity-norm of the distal links' angular accelerations, respectively. The constraint of Eq. (43) was applied but the constraint on the velocity was modified to reduce gradually the velocity to zero when the joint length approached one of its limits:

$$\begin{cases} \left|\dot{\rho}_{ij}\right| \leq \dot{\rho}_{ij_{max}} & if \;\; \rho_{ij_{min}} + \rho_{delta} \leq \rho_{ij} \leq \rho_{ij_{max}} - \rho_{delta} \\ \left|\dot{\rho}_{ij}\right| \leq \frac{\dot{\rho}_{ij_{max}}}{\rho_{delta}}\left(\rho_{ij} - \rho_{ij_{min}}\right) & if \;\; \rho_{ij} < \rho_{ij_{min}} + \rho_{delta} \\ \left|\dot{\rho}_{ij}\right| \leq \frac{\dot{\rho}_{ij_{max}}}{\rho_{delta}}\left(\rho_{ij_{max}} - \rho_{ij}\right) & if \;\; \rho_{ij} > \rho_{ij_{max}} - \rho_{delta} \end{cases} \tag{46}$$

where ρ_{delta} defines the distance from the limit of the actuator length where the velocity starts decreasing.

The optimisation procedure is as follows for each step of the trajectory:

- for the specified pose, compute the coordinates of points B_i;
- compute the coordinates of A_i based on the values of optimisation variable ρ_{i1};
- numerically compute the velocities and accelerations of the base prismatic joints $\dot{\rho}_{i1}$ and $\ddot{\rho}_{i1}$;
- compute the velocities and accelerations of the distal prismatic joints using Eqs. (7) and (22), respectively;
- compute the angular accelerations of the distal links and the accelerations of the centres of mass of the cylinder and the piston of the distal links using Eqs. (26), (30) and (36), respectively,
- compute the required forces in the distal and base prismatic joints using Eqs. (39) and (41), respectively;
- minimise the objective function given in Eq. (45) while satisfying the constraints on the lengths (Eq. 43) and the velocities (Eq. 46);
- use the optimised value of ρ_{i1} at step k as the initial guess for the next step $k + 1$ of the trajectory.

Values of α = 1000 and b = 0.5 were used when computing the objective function of Eq. (46). The other variables that are used as constraints were given the values shown in Table 1.

Table 1. Constraints for PRPR manipulator simulations

$\rho_{ij_{max}}$	$\rho_{ij_{min}}$	$\dot{\rho}_{ij_{max}}$	ρ_{delta}
0.29 m	0.01 m	0.25 m/s	0.02 m

5 RESULTS AND DISCUSSION

A spiral trajectory was used to demonstrate the force optimisation capabilities. The non-redundant and redundant manipulators were compared to quantify the improvement. The base triangle for both manipulators has sides of length O_iO_j = 0.3 m. As for the end effector, the sides of the equilateral triangle are of length B_iB_j = 0.05 m. The dynamic parameters used for the simulation are shown in Table 2.

Table 2. Dynamic parameters

Mass (kg)	m_p	1.5
	m_1	0.5
	m_2	0.8
	m_3	0.5
Moment of Inertia (kg m^2)	I_2	0.005
	I_3	0.003
	I_p	0.0075
Centre of gravity of distal links (cylinder and piston) (m)	r_2	0.2
	L_3	0.3

The trajectory and the constant orientation workspace of the 3-RPR manipulator are shown in Figure 4. A 100 N force is acting at the centre of the end-effector in the direction opposite to its motion, i.e., tangent to its trajectory, and a counter clockwise moment of 10 Nm is also applied on the platform. The end-effector is kept at a constant orientation of π/6 rad. The velocity was set at 0.007 m/s, a value slightly larger than that used in [13] to increase the dynamic effects. With larger velocities, the optimisation was not able to satisfy the velocity constraints of the actuators.

The trajectory chosen is a logarithmic spiral described by the polar equation

$$\rho = ae^{k\beta} \text{ with } k = cot\psi \tag{47}$$

where ρ is the spiral radius for a given angle β, which varies from 0 to 2π for the trajectory shown in Fig. 4, a is a constant that was set to 0.03 m, and ψ represents the angle between the tangent and the radial line from the origin of the spiral, (-0.05, 0) m, to the radial point (ρ, β). The trajectory was chosen in order to cover a large portion of the workspace. This was done to display the advantages of the redundant manipulator when faced with near-singular end-effector configurations. Angle ψ was chosen as 75°. The wrench applied on the manipulator in this case is thus

$$\mathbf{F} = [-100\cos(\beta+\psi), -100\sin(\beta+\psi);\ 10]^{\mathrm{T}}\ \mathrm{N;Nm} \tag{48}$$

When the velocity is constant along the spiral, the elapsed time between two angular positions is not constant for a constant increment $\Delta\beta$. Since the velocity is constant, the elapsed time Δt between two angles β_{i-1} and β_i can be computed with

$$\Delta t = \frac{\Delta L}{V} = \frac{1}{V}\int_{\beta_{i-1}}^{\beta_i}\sqrt{\rho^2+\frac{d\rho}{d\beta}^2}\,d\beta = \frac{a\sqrt{1+k^2}}{kV}\left(e^{k\beta_i}-e^{k\beta_{i-1}}\right) \tag{49}$$

where ΔL is the length of the curve between the angles. This time is used to numerically compute the velocities and accelerations of the base prismatic joints of the redundant manipulator. Increments of π/200 were used. The time required to complete the trajectory at a constant velocity of 0.007 m/s is 72.6 s. The

range limits on the prismatic joints in Eq. (43) were set to 0.01 m to 0.29m, while the prismatic actuators were limited to ±0.25 m/s.

Figure 5 presents the actuator forces when the 3-RPR manipulator follows the spiral trajectory.

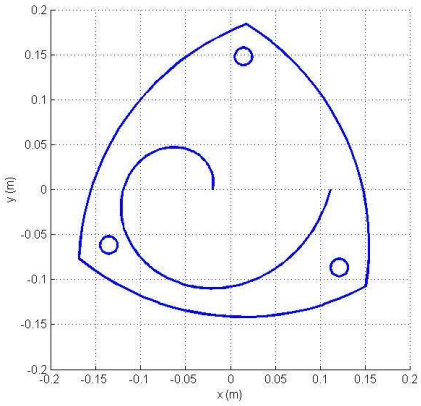

Fig. 4. Constant orientation ($\pi/6$) workspace of the 3-RPR and spiral trajectory

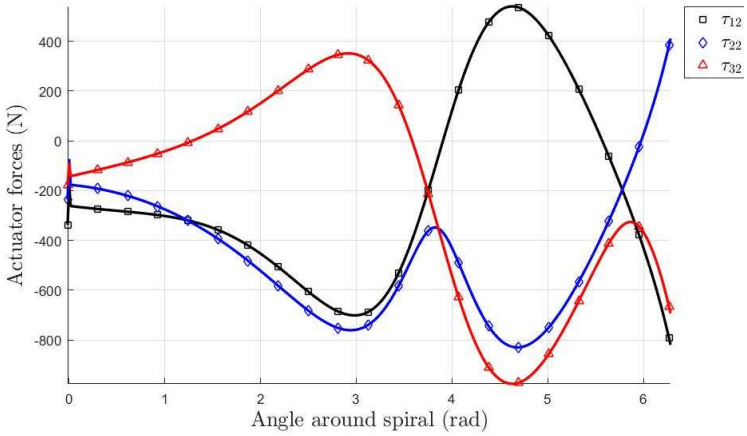

Fig. 5. Actuator forces for the 3-RPR manipulator for the spiral trajectory

To optimise the redundant manipulator, the initial start point $\mathbf{x}_o = [0.255, 0.212, 0.244]^T$ m was found using a PSO to minimise $\boldsymbol{\tau}^T\boldsymbol{\tau}$ at the initial pose. The initial start point has a significant effect on the optimised solution. Figure 6 presents the optimised results for the 3-PRPR manipulator following the spiral trajectory, in which the actuator lengths, actuator velocities and actuator forces of the manipulator are shown. A comparison of Figs. 5 and 6(c) clearly shows that the forces requires for the redundant manipulator are less than those for the non-redundant manipulator. The maximum forces for the redundant manipulator are less than half of the maximum forces for the non-redundant manipulator.

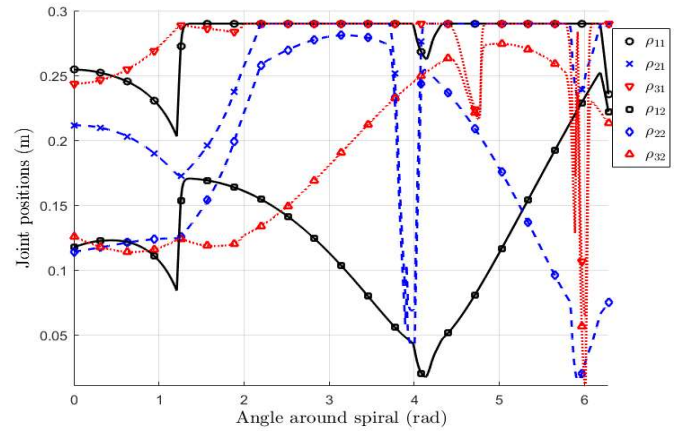

(a)

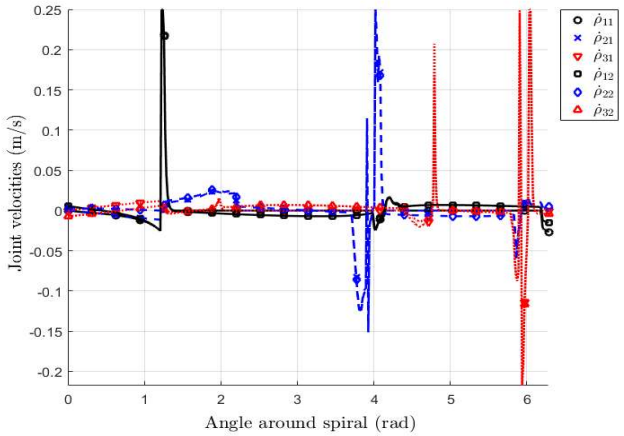

(b)

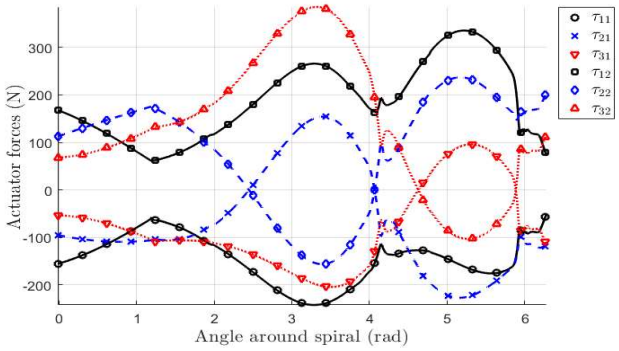

(c)

Fig. 6. (a) Actuator lengths, (b) actuator velocities and (c) actuator forces for the 3-PRPR manipulator for the spiral trajectory

As mentioned previously, the dynamic effects were included to verify if the kinetostatic approach used in [13] was valid. The maximum acceleration of the actuators (not shown) for the results shown in Fig. 6 is 2.85 m/s^2. Even if this acceleration is not that large, it was not obvious if some of the other components, for example the normal acceleration, could produce large forces that would significantly affect the required

forces in the actuators. Fig. 7 shows the actuator forces that are due to the dynamic effects only. A simulation was done setting the masses and moments of inertia to zero. The actuator forces due to the dynamic effects only are obtained by subtracting the forces obtained with zero mass from the forces obtained in Fig. 6c. Fig. 7 shows that the forces due to the dynamic effects are indeed negligible compared to the forces shown in Fig. 6c.

The results show that for this particular application the kinetostatic approach was valid. However, the dynamic effects would be important if the wrench applied on the end-effector were smaller or if the velocity of the end-effector were larger. If the constraints on the velocities of the actuators were relaxed, the dynamic effects would also increase. It should be noted that even if the inclusion of the dynamics does not significantly modify the results for the application studied here, it did however create difficulties during the optimisation. The objective function used in [13] produced large oscillations and unstable results when the dynamic equations were used in the optimisation.

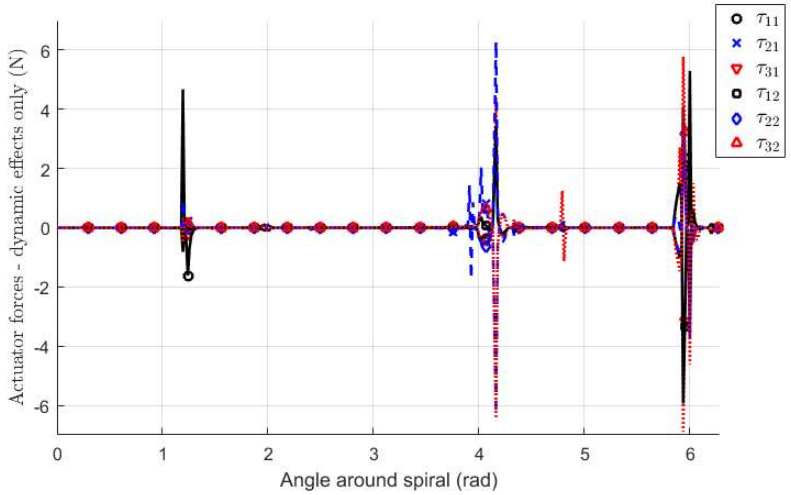

Fig. 7. Actuator forces due to dynamic effects for the 3-PRPR manipulator

6 CONCLUSIONS

The dynamic model of a kinematically-redundant planar parallel manipulator was presented and an optimisation approach was developed to minimise the actuator torques when following a specified trajectory. The results were compared with a non-redundant manipulator and with a kinematically-redundant manipulator using a kinetostatic approach. The results show that smaller torques are required by the redundant manipulator compared to those of the non-redundant manipulator. In addition to requiring smaller forces, it was shown in [13] that the kinematically-redundant manipulator can pass through configurations that are singular for the non-redundant manipulator.

The inclusion of the dynamic forces produced some undesirable oscillations if the same objective function that was used in the kinetostatic approach was used. A term had to be added to the objective function to limit the angular accelerations of the distal links to remove the oscillations. For the example studied here, the assumption that a kinetostatic approach could be used [13] proved to be valid. The decision to use a kinetostatic approach or to include the dynamics depends on the amplitude of the wrench applied on the end-effector, on the velocity of the end-effector and on the constraints on the velocities of the actuators.

ACKNOWLEDGEMENTS

The authors would like to thank the Natural Sciences and Engineering Research Council of Canada for their financial support for this work.

REFERENCES

1. Gosselin, C. and Angeles, J., "Singularity analysis of closed-loop kinematic chains," *IEEE Transactions on Robotics and Automation*, Vol. 6, No. 3, pp. 281–290, 1990.
2. Merlet, J.-P., "Redundant parallel manipulators," *Journal of Laboratory Robotics and Automation*, Vol. 8, No. 1, pp. 17–24, 1996.
3. Nokleby, S., Fisher, R., Podhorodeski, R. and F. Firmani, F., "Force capabilities of redundantly-actuated parallel manipulators," *Mechanism and Machine Theory*, Vol. 40, No. 5, pp. 578–599, 2005.
4. Firmani, F., Zibil, A., Nokleby, S.B. and Podhorodeski, R.P. "Force-moment capabilities of revolute-jointed planar parallel manipulators with additional actuated branches, " *Transactions of the Canadian Society for Mechanical Engineering*, Vol. 31, No. 4, pp. 469–481, 2007.
5. Zhao, Y. and Gao, F., "Dynamic formulation and performance evaluation of the redundant parallel manipulator," *Robotics and Computer-Integrated Manufacturing*, Vol. 25, No. 4-5, pp. 770-781, 2009.
6. Wang, J. and Gosselin, C.M., "Kinematic analysis and design of kinematically redundant parallel mechanisms," *ASME Journal of Mechanical Design*, Vol. 126, No. 1, pp. 109–118, 2004.
7. Mohamed, M. G. and Gosselin, C. M., "Design and analysis of kinematically redundant parallel manipulators with configurable platforms," *IEEE Transactions on Robotics*, Vol. 21, No. 3, pp. 277–287, 2005.
8. Ebrahimi, I., Carretero, J. A. and Boudreau, R., "3-PRRR redundant planar parallel manipulator: inverse displacement, workspace and singularity analyses," *Mechanism and Machine Theory*, Vol. 42, No. 8, pp. 1007–1016, 2007.
9. Ebrahimi, I., Carretero, J. A. and Boudreau, R., "Kinematic analysis and path planning of a new kinematically redundant planar parallel manipulator," *Robotica*, Vol. 26, No. 3, pp. 405–413, 2008.
10. Cha, S.-H., Lasky, T. A. and Velinsky, S. A., "Kinematically-redundant variations of the 3-RRR mechanism and local optimisation-based singularity avoidance," *Mechanics Based Design of Structures and Machines*, Vol. 35, pp. 15–38, 2007.
11. Cha, S.-H., Lasky, T. A. and Velinsky, S. A., "Determination of the kinematically redundant active prismatic joint variable ranges of a planar parallel mechanism for singularity-free trajectories," *Mechanism and Machine Theory*, Vol. 44, No. 5, pp. 1032–1044, 2009.
12. Kotlarski, J., Thanh, T. D., Heimann, B. and Ortmaier, T. "Optimisation strategies for additional actuators of kinematically redundant parallel kinematic machines," *Proceedings of IEEE Conference on Robotics and Automation*, Anchorage, USA, pp. 656–661, May 3–8, 2010.
13. Boudreau, R. and Nokleby, S., "Force optimisation of kinematically-redundant planar parallel manipulators following a desired trajectory," *Mechanism and Machine Theory*, Vol. 56, No. 10, pp. 138–155, 2012.
14. Ruggiu, M. and Carretero, J. A., "Kinematic analysis of the 3-PRPR redundant planar parallel manipulator," *Proceedings of the 2009 CCToMM Symposium on Mechanisms, Machines, and Mechatronics*, Québec, Qc, Canada, May 28-29, 2009.
15. Guo, D. and Zhang, Y., "Different-level two-norm and infinity-norm minimization to remedy joint-torque instability/divergence for redundant robot manipulators," *Robotics and Autonomous Systems*, Vol. 60, No. 6, pp. 874-888, 2012.